



# All-atom molecular dynamics simulations of lung surfactant protein B: Structural features of SP-B promote lipid reorganization



Mohammad Hassan Khatami<sup>a</sup>, Ivan Saika-Voivod<sup>a</sup>, Valerie Booth<sup>a,b,\*</sup>

<sup>a</sup> Department of Physics and Physical Oceanography, Memorial University of Newfoundland, St. John's, NL A1B 3X7, Canada

<sup>b</sup> Department of Biochemistry, Memorial University of Newfoundland, St. John's, NL A1B 3X9, Canada

## ARTICLE INFO

### Article history:

Received 11 May 2016

Received in revised form 30 August 2016

Accepted 20 September 2016

Available online 23 September 2016

### Keywords:

Lung surfactant protein

SP-B

POPC

GROMACS

Molecular dynamics

Bilayer diffusion

## ABSTRACT

Lung surfactant protein B (SP-B), a 79 residue, hydrophobic protein from the saposin superfamily, plays an essential role in breathing. Because of the extreme hydrophobicity of SP-B, the experimental structure of this protein has not yet been determined. Here, we run all-atom molecular dynamics simulations using the OPLS-AA force field in GROMACS to study SP-B's structure and mechanisms for promoting lipid reorganization. Firstly, we find that the final structures indicate the need for some fine-tuning of the homology-based secondary structure predictions. Secondly, we find energetically feasible structures 1) with SP-B's helices in the plane of the bilayer, 2) with SP-B's helices inclined with respect to the bilayer, and 3) with SP-B in a closed structure interacting peripherally with the bilayer. Interestingly, SP-B structures that were bent at the hinge region between the pairs of helices promoted and/or stabilized defects in the lipid bilayer. Finally, particular salt bridge patterns and structural plasticity in the central loop and adjacent region of SP-B appeared to be involved in SP-B's lipid reorganization abilities.

© 2016 Elsevier B.V. All rights reserved.

## 1. Introduction

Lung surfactant (LS) is a complex mixture of proteins and lipids that covers the air–water interface of the alveoli, where it reduces surface tension and helps us breathe. By weight, 80–85% of human lung surfactant is phospholipids, 5–10% neutral lipids and ~10% proteins [1,2,3]. About 80% of the phospholipids are phosphocholine (PC) lipids, half of which are dipalmitoylphosphatidylcholine (DPPC). Along with PC lipids, there is a significant amount of phosphatidylglycerol (PG) lipid. The protein complement of lung surfactant is composed of pulmonary surfactant proteins SP-A, SP-B, SP-C and SP-D [4]. The hydrophilic surfactant proteins, SP-A and SP-D, contribute to immune functions within alveoli [5,6], while the hydrophobic surfactant proteins (SP-B and SP-C) modulate the surface activity of LS lipids, easing the breathing process [7,8]. Among these proteins, SP-B is the essential protein for life [9].

SP-B is a 79 residue protein from the saposin super family whose members share a structure with 3 internal disulfide bonds linking 4–5

helical regions. Several experimental structures of proteins from the saposin super family have been determined [10,11,12,13,14,15,16,17,18]. While these saposin super family structures display similar secondary structure and internal disulfide bonds, there is a great deal of variation in their tertiary structures; some of the structures are compact and closed, while others form open structures with a large, exposed hydrophobic surface that can have extensive interactions with lipids. It is not known if SP-B forms an open, closed, or intermediate overall structure.

SP-B is substantially more hydrophobic than other saposin super family members [19], which has meant that thus far, it has proven recalcitrant to structure determination. The largest fragment of SP-B for which there is an experimentally determined structure, is termed Mini-B [20] and encompasses an N-terminal and C-terminal helix of SP-B linked by 2 disulfide bonds (Fig. 1).

In addition to the 6 cysteine residues conserved in the saposin superfamily, SP-B has a 7th cysteine (C48) that has been widely assumed to stabilize an SP-B dimer. However, SP-B purified from animal lungs exhibits a variety of oligomeric states and deletion of C48 does not drastically impair SP-B's function [21]. It has been suggested that, in addition to a C48–C48 disulfide bond, SP-B dimers may be stabilized through salt bridges between E51 and R52 [22,23]. Olmeda et al. [24] have recently proposed that SP-B acts as a multimer of dimers, forming hydrophobic ring/tube shapes. Thus, SP-B's functional oligomerization state is still something of an open question. Another structural feature of SP-B that is not present in other saposin super family proteins is the N-terminal 7-residue “insertion sequence”, which has been proposed to help SP-B insert into lipid bilayers [25].

**Abbreviations:** SP-B, surfactant protein B; LS, lung surfactant; PC, phosphocholine; DPPC, 1,2-dipalmitoyl-sn-glycero-3-phosphocholine; PG, phosphatidylglycerol; POPC, 1-palmitoyl-2-oleoyl-sn-glycero-3-phosphocholine; AA, all-atom; CG, coarse-grained; MD, molecular dynamics; GROMACS, GROMINGEN MACHINE for Chemical Simulations; OPLS-AA, Optimized Potentials for Liquid Simulations-All Atom; BLAST, basic local alignment search tool; STRIDE, STRuctural IDentification; VMD, Visual Molecular Dynamics; DSSP, Define Secondary Structure of Proteins; PDB, Protein Data Bank; SPV, Swiss PDB viewer.

\* Corresponding author at: Department of Biochemistry, Memorial University of Newfoundland, St. John's, NL A1B 3X9, Canada.

E-mail address: [vbooth@mun.ca](mailto:vbooth@mun.ca) (V. Booth).

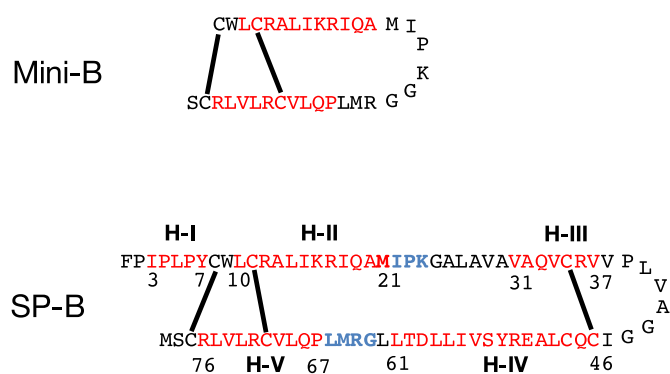


**Fig. 1.** Amino acid sequence of SP-B and Mini-B. Red residues indicate helical regions, which have been determined experimentally for Mini-B. For SP-B, the secondary structure indicated is for the initial models used in the MD. Heavy lines indicate disulfide bonds. Blue residues indicate the “hinge” that we bend to generate the initial open, V-shaped, and closed SP-B structures. Details of how SP-B’s secondary structure was defined can be found in the Methods section. (For interpretation of the references to color in this figure legend, the reader is referred to the web version of this article.)

Investigations into SP-B’s mechanism of action have resulted in a list of *in vitro* activities for SP-B: membrane binding, membrane lysis, membrane fusion, promotion of lipid adsorption to air–liquid interfaces, stabilization of monomolecular surface films, and respreading of films from a collapsed phase [8]. However, without an experimental structure, a detailed understanding of SP-B’s mechanism for these activities is lacking. Several researchers have employed computational approaches to predict the structure and behavior of SP-B in lipid bilayers. Zaltash et al. [22] have employed Monte Carlo simulations to investigate SP-B’s monomeric and dimeric structures, using NK-lysin as a template for the secondary structure of the SP-B. Based on their model, they have predicted that the distribution of polar and non-polar residues in the SP-B dimer is compatible both with SP-B positioning at the water–lipid interface of a bilayer and with the ability of SP-B to cross-link membrane multilayers. Baoukina and coworkers have performed coarse grained simulations of monomers of SP-B and SP-C interacting with vesicles. They have studied SP-B promoted membrane fusion [26,27], which they did while holding the secondary structure of SP-B fixed.

With this work, we employ all-atom MD simulations to find and detail feasible low energy structures for SP-B and to indicate how particular features of secondary and tertiary structure affect SP-B’s ability to promote non-lamellar lipid structures. To this end, we build six different SP-B/lipid systems with almost 200,000 atoms each, and simulate these systems for more than 2  $\mu$ s. The simulations give us detailed information about the structure and lipid interactions of SP-B and provide detailed hypotheses for the structural mechanism of the protein.

## 2. Methods

### 2.1. Initial SP-B structure

In order to start with the best SP-B structure possible, we took into account the experimentally determined structures of SP-B fragments, as well as secondary structure prediction based on homology modeling, and we also kept in mind the structures employed in previous simulation work with SP-B. Running the basic local alignment search tool (BLAST) [28] on the UniPort webpage (<http://www.uniprot.org/blast/>) indicates the closest template for SP-B is Saposin C, with only ~25% sequence identity. However, the homology model of SP-B based on the Saposin C crystal structure (PDB ID: 2QYP [18]) produces ~82% helicity, which is much higher than the experimental values for SP-B (35–50% [19]), and also does not match the experimental structures of SP-B fragments, including Mini-B. On the other hand, the SP-B homology model

based on NK-lysin (PDB IDs: 1NKL [14]), which has ~18% sequence identity to SP-B, produced a better match to the overall secondary structure of SP-B, as well as the helical regions of Mini-B. Thus, the NK-lysin model was chosen as the basis for the starting secondary structure employed for the regions of SP-B that do not have an experimental structure (Helices III and IV). Note that standard methods of secondary structure prediction (e.g. JPred4 [29,30]) were not employed because they predict much higher levels of helical structure than is observed experimentally for SP-B and also fail to position the cysteine residues so that the known disulfide bonds can be formed.

The initial SP-B model was constructed using Swiss PDB viewer (SPV) software [31] by starting with the experimental structure for Mini-B, PDB ID: 2DWF [20] (Helices II and V in Table 1), and building on the rest of the protein. Residues 1–7 are not homologous to any other saposin proteins and so this region was allowed to take on the default structure generated by SPV – i.e. helical (Helix 1 in Table 1). Residues 25 to 62, which contain helices III and IV, were built in using the SPV “add residue” build option and the secondary structure of each residue set based on the NK-lysin homology model. We made our SP-B protein in two different structures, open and bent (V-shape) (Fig. 2). The regions at the bend were chosen to be Met-21 to Lys-23 and Gly-63 to Leu-66 in order to preserve the helical regions. In Table 1 we compare the helical regions of our model (calculated as described in Section 2.3) (Fig. 1) to other models previously generated for SP-B [26, 27,32,33]. The main differences between our model and the rest of the models in Table 1 are the addition of Helix-I (residues 3–7) in the N-terminus and the position of Helix-IV (residues 46–61), where we remove the helical structure of the G43–G44 pair.

### 2.2. Initial lipid bilayer structure

In setting up our simulations, we used a pre-assembled POPC bilayer composed of 512 lipid molecules. The bilayer employed had a pore so that lipid molecules could move from one leaflet to the other, in order to keep the lipid/area ratio in the whole bilayer constant. To generate the bilayer, we started with 3 pre-assembled perfect lipid bilayers, each composed of 128 lipid molecules, and one lipid bilayer containing a pore, also composed of 128 POPC lipids (from one of our control simulations in our previous publication [34]). We put these four bilayer sections beside each other in a square to produce our lipid bilayer containing 512 POPC lipid molecules. To equilibrate the new lipid bilayer, we added water to the system and ran it under NVT conditions for 2 ns at 310 K, and subsequently under NPT conditions for 50 ns at 310 K. The pore in the initial bilayer remained for the duration of the simulation as previously observed [34].

### 2.3. Generation of SP-B/POPC systems

Next, we added protein to the system. For each of the protein structures (open and bent) we put the protein in three different positions with respect to the bilayer: inside (in), half-inside (half) and outside (out) the bilayer (Fig. 2). In all cases we positioned the hydrophobic

**Table 1**

Proposed helical regions, given by residue number, of SP-B in different models. The open and bent structures for the all-atom force field are the two models we use in our simulations. The previously used models are Model-A, introduced by Baoukina and coworkers [26,27], Model-B, which was a secondary structure model previously used in our group [32], and model-C, introduced by the Johansson group [33].

Helical region	Open model	Bent model	Model-A	Model-B	Model-C
Helix-I	3–7	3–7	–	–	–
Helix-II	10–21	10–20	7–21	10–20	8–22
Helix-III	31–37	31–37	32–36	26–35	27–38
Helix-IV	46–61	46–62	42–64	44–58	42–50
Helix-V	67–76	67–76	68–76	67–78	67–74

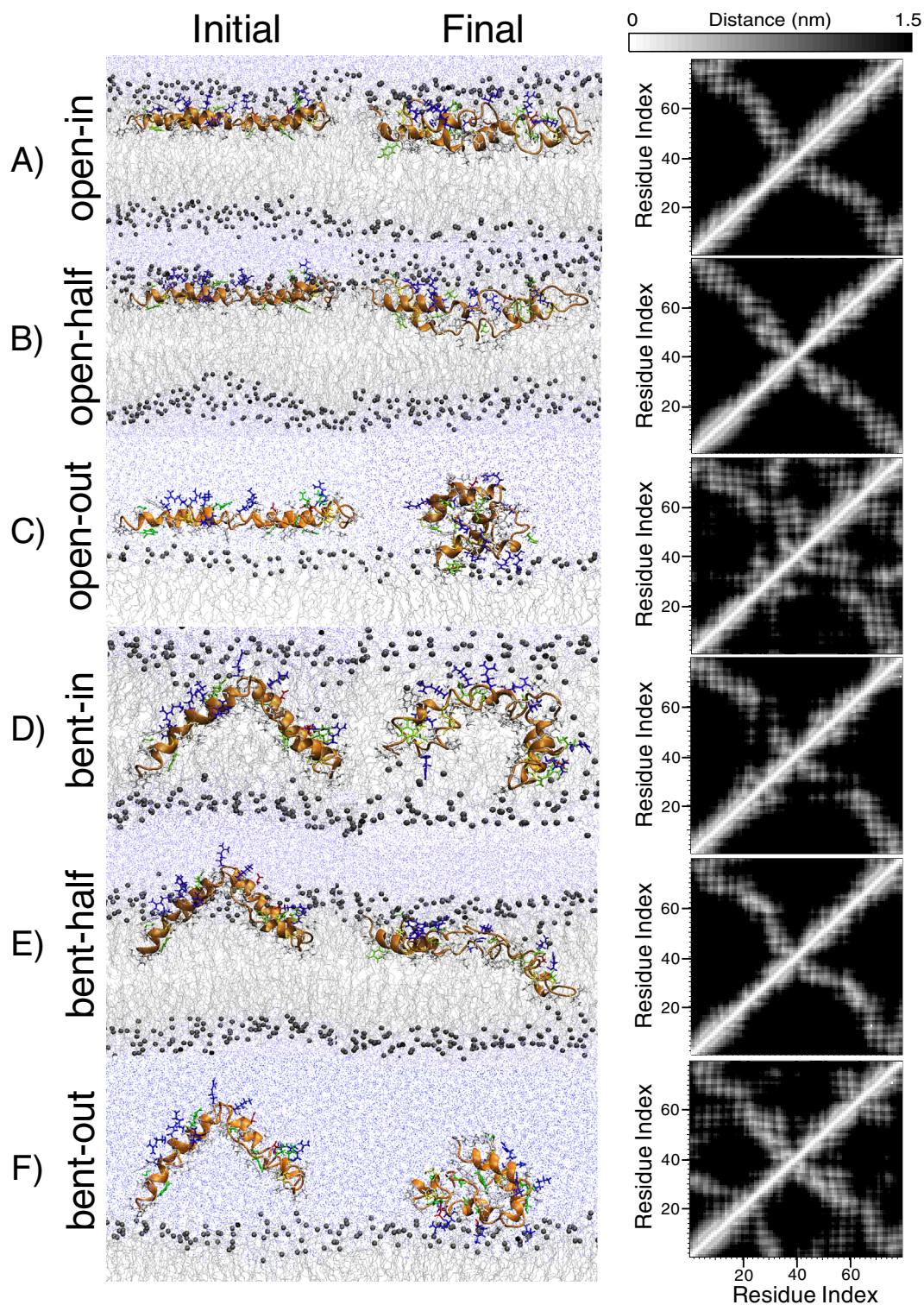


**Fig. 2.** (A–F) Snapshots of initial (left) and final structures (middle), as well as average residue-to-residue distance over the last 200 ns (right) of A) open-in, B) open-half, C) open-out, D) bent-in, E) bent-half and F) bent-out simulations. In A–F (left and middle), hydrophobic sidechains (white colored) initially face toward the lipid bilayer center, while the hydrophilic sidechains (colored) face toward the water molecules (blue dots). On the right column, we can see open-in, open-half and bent-half systems have similar distance plots, indicating similar overall protein structures in these simulations. The brighter the color, the smaller the average distance between the residues. (For interpretation of the references to color in this figure legend, the reader is referred to the web version of this article.)

face of the protein towards the bilayer center and the hydrophilic face towards the water. SP-B was placed far from the (preformed) pore to prevent the protein from interacting with the pore. To insert the protein inside the bilayer, we used the *g\_membed* [35] tool in GROMACS, which embeds a protein in a lipid bilayer by removing the minimum number

of lipid molecules. Each of our six simulation boxes generated in this way had 496 POPC lipid molecules, 38,000 TIP4P water molecules, 7  $\text{Cl}^-$  counter ions and an SP-B protein. The system size in X, Y and Z directions before starting the simulation was ~12.4 nm, ~12.3 nm and ~11.7 nm, respectively.

## 2.4. Molecular dynamics

In carrying out MD simulations we used the OPLS-AA force field [36, 37] adapted for POPC lipid molecule properties [38]. For each of the simulation boxes we used the same method to set up and run the simulations. In the first step, under NVT conditions we ran the system at 310 K for 2 ns with the protein position restrained and a time step of 2 fs. We kept the protein position restrained to prevent any structural changes before the production run. In the second step, we ran the system under NPT conditions at 310 K and 1 atm for 100 ps, with protein position restrained and Parrinello-Rahman isotropic pressure coupling with  $\tau_p = 5$  ps and compressibility  $= 4.5 \times 10^{-5} \text{ bar}^{-1}$ . In the production run we simulated the system under NPT conditions at 310 K and 1 atm, using Parrinello-Rahman semi-isotropic pressure coupling, with the same time constant and compressibility as the earlier steps, but without the protein position restraints. We ran these simulations with a time step of 2 fs for 2 to 2.5  $\mu\text{s}$  in duration, except for the bent-out simulation, which we ran for only 700 ns because the protein quickly forms a closed, stable structure.

## 2.5. Simulation analysis

We used GROMACS tools, as well as the STRIDE and salt bridge plugins of VMD 1.9.1 [39,40] to analyze the simulation results. We tried both STRIDE [41] as a VMD plugin and DSSP [42,43] as a GROMACS tool, to calculate the secondary structure of SP-B. These methods use two different ways of calculating the secondary structure. Although employing both methods gave similar results, there were differences between them, e.g. in the initial structure of SP-B C46-G47-C48 were defined to be in  $3_{10}$  helical structure by the STRIDE plugin of VMD, while the DSSP plugin of GROMACS called this region  $\alpha$ -helical. Thus, we called both  $\alpha$ -helical and  $3_{10}$ -helical secondary structures with the general name of “helical” structure. We used VMD 1.9.1 to visualize our system.

## 3. Results

We have performed all-atom simulations of SP-B in a POPC bilayer (Table 2), with the initial SP-B structure based in part on homology modelling and in part on the experimental structure of Mini-B (Fig. 1 and Table 1). We generated the SP-B structure in two initial conformations: open and bent (V-shape) and placed each of these two starting structures at three initial positions with respect to the lipid bilayer: outside, half-inside and inside (Fig. 2, left-hand column).

### 3.1. System evolution during simulation

Despite the long run times, we see from the plots of the potential energy (Fig. 3) that the systems are still relaxing. However, the nearly steady-state behavior of the radius of gyration (Rg) of the protein's backbone (Fig. 3) as well as the helicity (Fig. S.1) and the SP-B to membrane distance (Fig. S.2), and the small root mean square deviation (RMSD) values attained at the longer times (Fig. 3) indicate that each of the simulations is converging to an equilibrium state. Here, we note that the energy plots are comparable to each other because care was taken to keep identical system compositions. Small differences in the

initial values of the radii of gyration within the bent and open SP-B systems are due to small changes in protein structure that arise during preparation of the simulation box. The final Rg values for each simulation (Fig. 3) correlate well to the relative compactness of the protein as seen in the final snapshots in Fig. 2 (center column). In addition to the Rg plots, the RMSD plots (Fig. 3) show that each system has reached an RMSD value of  $<2 \text{ \AA}$ , a value often taken to indicate that the system has reached an equilibrium state (Fig. 3) [44,45]. Note that while five of the simulations were run out to 2000 ns or more, one of the runs, the bent-out, was run only to 700 ns, because it reaches a metastable state quickly, as judged by an RMSD value of  $<2 \text{ \AA}$  and a similar Rg value to the other out structure in our simulations, i.e. open-out.

### 3.2. SP-B structure

Visual inspection of the final structures of the protein in the open-in, open-half, and bent-half simulations, and similarities in residue-residue distance plots (Fig. 2-A, B and E) indicate at least partial convergence of SP-B's structure in these three simulations, although the bent-half system has a different final orientation in the lipid bilayer compared to the open-in and open-half systems. In these three simulations, SP-B takes on an extended structure with the N- and C-terminal helices positioned parallel to the bilayer surface. The central helix pair are located in the same bilayer leaflet, for the open-in and open-half systems, but are in contact with the opposing leaflet in the bent-half system. By contrast, in both the open-out (Fig. 2-C) and bent-out (Fig. 2-D) simulations we can see that SP-B takes on a closed globular structure. The closed structures interact with lipid bilayer headgroups via either hydrophilic side of the structure, i.e. through middle helices (Helix-III and IV) in the open-out system (Fig. 2-C) and through terminal helices (Helix-I, II and V) in the bent-out system (Fig. 2-F). It is interesting to note that the closed structure that forms from the open-out simulation, does so through a rather non-trivial sequence of configurational changes during the course of roughly 1.5  $\mu\text{s}$ . The final structure in the remaining simulation, bent-in, (Fig. 2-D) presents an overall structure that is intermediate in compactness compared to the open final structures (in Fig. 2-A, B, and E) and closed structures (in Fig. 2-C and F). The bent-in (Fig. 2-D) and bent-half (Fig. 2-E) simulations display interesting lipid interactions that will be discussed below.

Moving from overall structure to secondary structure, Fig. 4 (Panels A and B) presents the average helicity ( $\alpha$ -helix plus  $3_{10}$  helix) for each SP-B residue, as well as the overall percent helicity versus time (Fig. 4-C and D) over the last 200 ns of simulations. The plots indicating full time overall percent helicity versus time are available as Fig. S.1 in supplementary data. The initial helicity of the starting SP-B structures is indicated by the shaded background (Fig. 4-A and B) and the large black dot (Fig. 4-C and D). In all the simulations, the overall helicity of the protein remains almost constant during the last 200 ns, indicating that SP-B is near to an equilibrium state in terms of the secondary structure. Reassuringly, the final mean value of overall helicity of  $\sim 35\%$  is similar to the experimentally observed secondary structure of SP-B [19]. This final helicity is substantially lower than the helicity of the initial starting structures of SP-B that we had built.

The initial SP-B structure had 5 helices: helix-II and V, based on the Mini-B experimental structure; helix III and IV based on homology modeling; and helix I at the N-terminus, for which little structural data is available, but which was set as a helical region as the default for the software used to build the structure (Figs. 1 and 4, and Table 1). Interestingly, the helix-I and helix-II regions partially merge into each other in all but the open-out system, where the protein has a clear boundary between helix-I and helix-II. This suggests that despite the prolines at residues 2, 4 and 6, a largely helical secondary structure is still feasible for this region of SP-B when it is in contact with lipids. Helix-V, which was initially based on the experimental Mini-B structure, is well preserved in our simulations, which supports a similar

**Table 2**  
Brief summary of each simulation.

System	Time (ns)	Description of protein behavior
Open-in	2000	Stable structure; similar initial and final depth in bilayer
Open-half	2000	Stable, but embeds to similar depth as open-in
Open-out	2500	Forms closed structure after large structural changes
Bent-in	2500	Relaxes, but maintains contact with initial defect in bilayer
Bent-half	2500	Induces pore formation; V-shape partially opens up
Bent-out	700	Protein closes rapidly

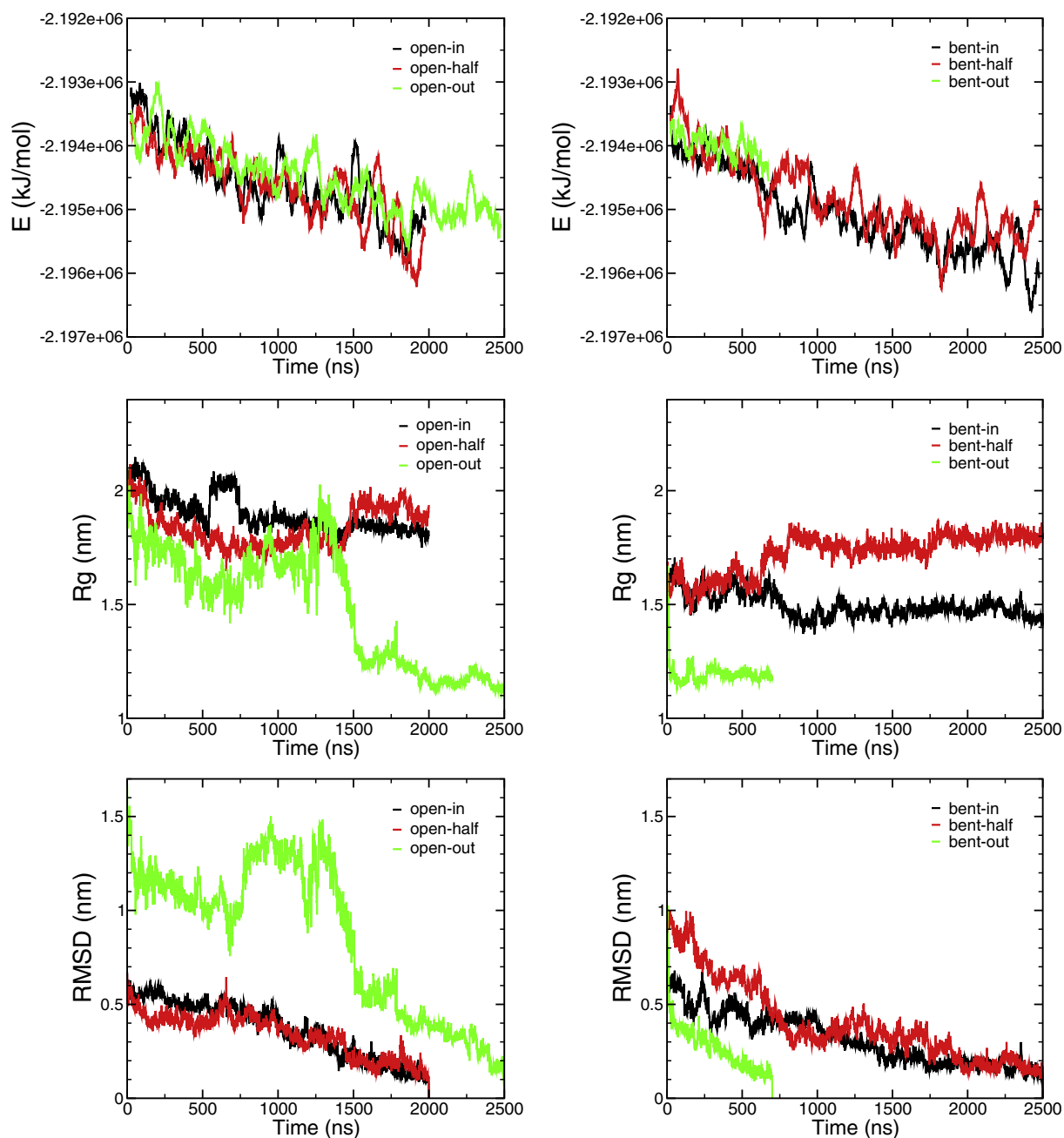


**Fig. 3.** Time evolution of the potential energy (top), radius of gyration (middle) and RMSD (bottom) of open (left) and bent (right) systems in the simulations. In the potential energy panels, the plots show running averages over 50 data points, with 1 ns between data points. We have used the heavy atoms of the main chain of SP-B to calculate  $R_g$  and RMSD, with 1 ns between data points.

structure for this region of SP-B in the context of the full length protein. Helix-III retains about 60% helicity on average when the protein is initially inside or half-inside the lipid bilayer (open-in, open-half, bent-in, bent-half). By contrast, the helicity is completely lost when this region is in a water environment (open-out and bent-out). In 5 out of 6 simulations, helix-IV divides into two smaller helical regions. When the protein is initially placed inside or half-inside the bilayer, the Arg-52, Tyr-53 region of the protein loses its helical structure in three of the four simulations. The exception is the open-half simulation, which could be altered due to the presence of salt bridges in this system, as discussed in the salt bridges section below. Thus, despite what the homology modeling predicted for the initial structure, residues 52 and

53 appear unlikely to take on a helical structure when SP-B is in contact with a lipid bilayer.

### 3.3. SP-B-lipid interactions

In Fig. 2 we can see snapshots of initial and final structures of SP-B in the POPC lipid bilayer. In all of these simulations, the protein structure and lipid interactions adapt in such a way that the charged residues are proximal to lipid head groups and/or water molecules. For the systems where SP-B is initially outside the bilayer (Fig. 2-A and F), the protein rapidly collapses into a compact structure with hydrophobic residues inside and the charged residues maintaining a peripheral

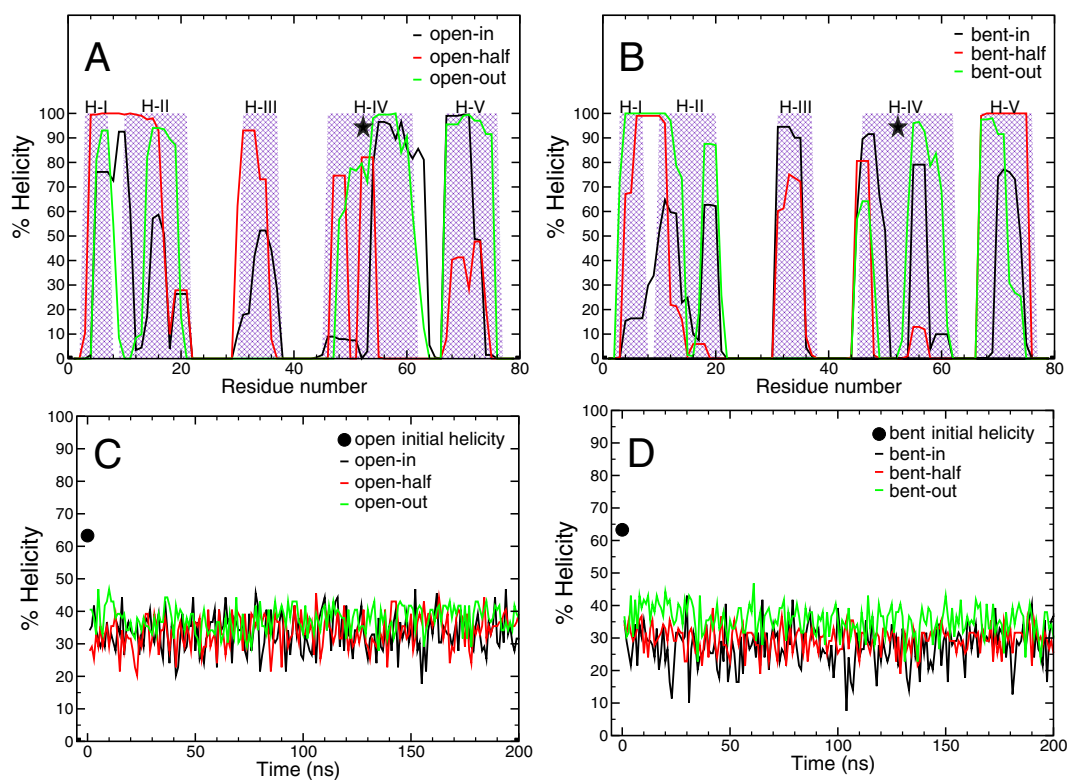


**Fig. 4.** Evolution of percent helicity of SP-B for each residue (A and B) and time evolution of percent helicity of SP-B (C and D) during the last 200 ns of simulations. We have used the STRIDE plugin of VMD to calculate the helicity, with 1 ns between data points. The hatched background in panel A and B and large black dot in panels C and D represent the helicity percent in the initial structure, calculated from the structure of SP-B after applying the force field in the first step of setting up the simulation in GROMACS, i.e. before the structure was subjected to all the pre-production run set-up steps. The black star in H-IV region of A and B indicates the position of residues 52–53. (For interpretation of the references to color in this figure legend, the reader is referred to the web version of this article.)

interaction with the lipid bilayer. The SP-Bs in the open-half and open-in simulations (Fig. 2-A and B) converge to a similar depth within one leaflet of the bilayer and have little, if any, interaction with the other leaflet. The bent-in and bent-half configurations (Fig. 2-D and E) are particularly

interesting as they illustrate how SP-B may be able to carry out the lipid re-organization activities thought to be at the heart of its mechanism.

In the bent-in simulation, SP-B remains inside the lipid bilayer, preserving a water-containing defect that was included initially as an

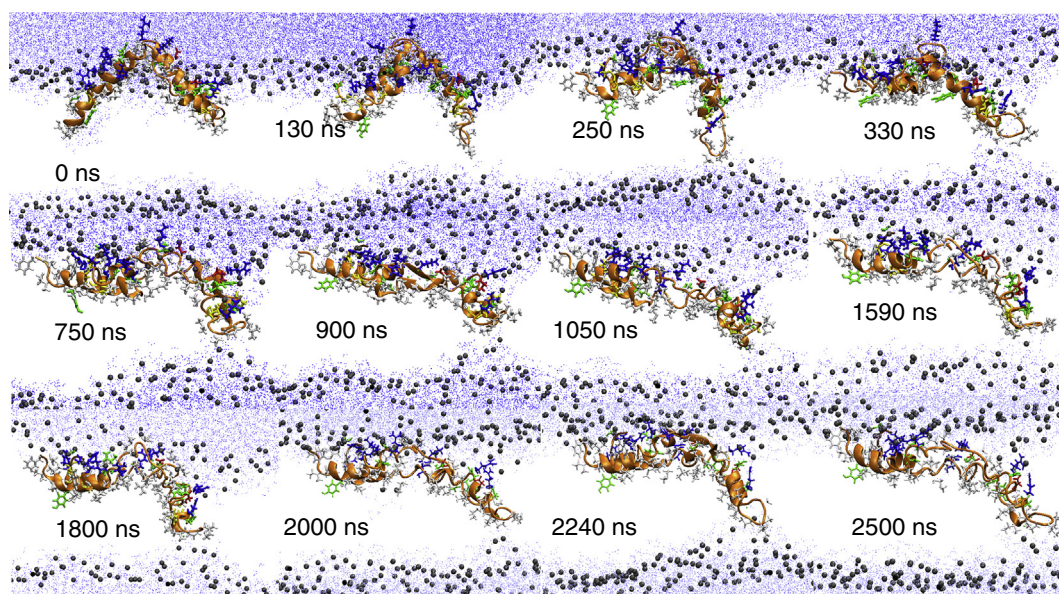


**Fig. 5.** Snapshots of bent-half system during the simulation. We can see protein initially has a V-shaped structure, placed half-inside the lipid bilayer. Hydrophobic sidechains (white colored) face towards the center of the bilayer, while the hydrophilic sidechains (colored) face towards the water molecules. We can see during the simulation that the Mini-B region of SP-B moves toward the lipid-water interface, parallel to the lipid bilayer, while the central segment of SP-B (the non-Mini-B part) reaches the other leaflet and produces a water-lined defect in the bilayer. During the simulation, we can see changes to the secondary (e.g.  $\beta$ -strands at  $t = 900$  ns) and tertiary structure of the protein. (For interpretation of the references to color in this figure legend, the reader is referred to the web version of this article.)

artifact of embedding the protein in the bilayer during the system set-up (Fig. 2-D). The initially sharply V-shaped structure of the protein softens during the simulation, to form a more continuous curve. Unlike the bent-in simulation, in the bent-half simulation, there is no defect in the original system set-up but SP-B appears to induce the formation of a defect during the course of the simulation (Figs. 2-E and 5). The defect formation is initiated when the loop between helices III and IV (VVPLVAGG) makes contact and then embeds in the opposing leaflet of the bilayer, which induces the formation of a pore (Fig. 5). Since proline is the only polar sidechain in the loop and is also considered a “disorder-promoting” amino acid, our analysis of this loop/lipid interaction centers on Pro-39. Fig. 6-A tracks the position of Pro-39 with respect to the lipid bilayer during the simulation. We can see Pro-39 travel from the upper leaflet to the lower leaflet, with a concomitant thinning of the bilayer in the region of both leaflets that are proximal to the proline.

In Fig. 6-B we can see the changes in the order parameter of the lipid acyl-chains with respect to the bilayer normal for the lipids in both leaflets that are proximal to the loop. Although there is no direct point-to-

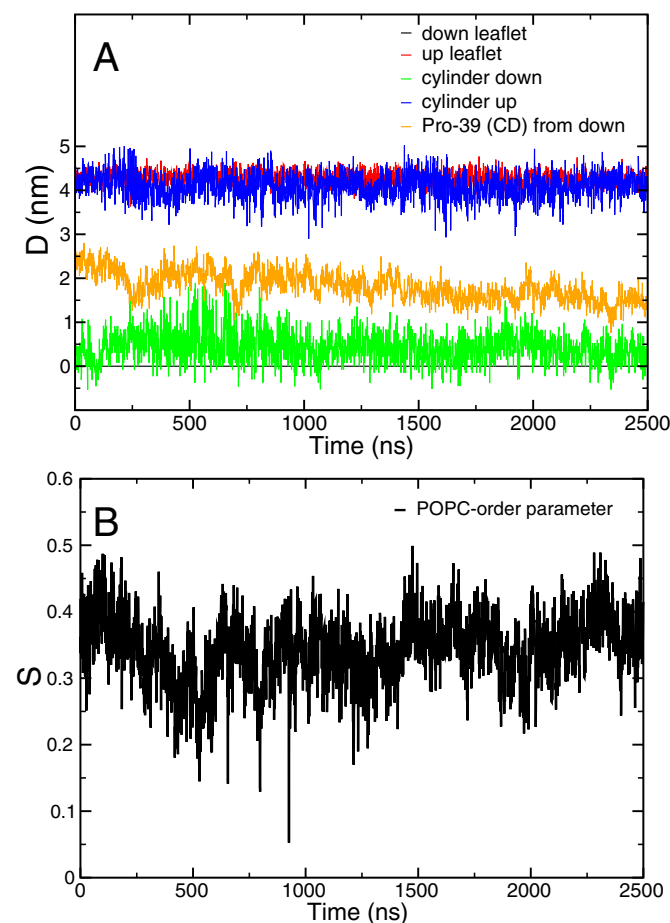


**Fig. 6.** Position of Pro-39 with respect to the lipid bilayer (A) and average order parameter of the lipid acyl-chains (B) in bent-half system during the simulation. In (A) the black and red colors represent the average position of bottom and top leaflets of the membrane, respectively. The blue and green colors represent the positions of the phosphorus atoms located within a cylinder (parallel to the bilayer normal) of radius 2 nm around the  $C_{\alpha}$  carbon atom of the Pro-39 residue, as well as the position of that carbon atom itself (orange). This carbon atom tracks the action of the proline residue within the loop region as it takes part in forming the defect, and the time series shows instances of dipping down towards the bottom leaflet before progressing continuously closer to the bottom leaflet, and stabilizing the pore formed (see also Fig. 5). In (B) the order parameter is calculated for lipid molecules with their head group within the 2 nm radius of a cylinder parallel to bilayer normal with  $C_{\alpha}$  of Pro-39 in the center. (For interpretation of the references to color in this figure legend, the reader is referred to the web version of this article.)

point relation apparent between the changes in the depth of the loop part of the protein (Fig. 6-A) and the order parameter of the acyl-chains (Fig. 6-B), we can see that during the penetration of the lipid bilayer (0 to  $\sim 1 \mu\text{s}$ ), the order parameter of the acyl-chains displays greater fluctuations. Correspondingly, when the protein is in a stable position in the lipid bilayer, the fluctuations in the order parameter decrease.

### 3.4. Salt bridges

There are intra-protein salt bridges (Fig. 7) present in the simulations of SP-B in POPC and they may play important roles in stabilizing SP-B's secondary and tertiary structures, as well as in SP-B's lipid interactions. The timescale for formation of the salt bridges during the simulation was quite variable, with some bridges forming within nanoseconds and others taking microseconds to form. In Fig. 7, we show a summary of the location of intra-protein salt bridges for the last 200 ns of the simulations for the runs with SP-B initially placed inside and half-inside the lipid bilayer.

One salt bridge of particular interest is between K24 and D59 (Fig. 7, red), which bridges the “hinge”, i.e. the apex of the V in SP-B's bent structure (Fig. 7, grey arrow). This salt bridge is present in the bent structures, but not in the open ones, which suggests that it might stabilize the bent configuration of SP-B. Also of note is the variability of the salt bridges involving residues E51 and R52 (Fig. 7, pink, green and brown), which correlates with the secondary structure variability observed in this region. For example, it appears that the salt bridge from R52 to D59 (Fig. 7, brown) stabilizes helical structuring of residues 52 and 53. This E51/R52 region is proximal to the central SP-B loop (Fig. 7 grey-dashed line) observed to make contact with the opposing bilayer leaflet in the bent-half simulation (Figs. 5 and 6). Thus, salt bridges may contribute to structural plasticity in this region that may be important for SP-B to penetrate the opposing lipid leaflet and induce the formation of a pore. Since anionic lipids are present in lung surfactant, there will be competition between lipid-protein and protein-protein salt bridges, and thus salt bridging may provide a mechanism for the local lipid composition to affect SP-B structure and SP-B-lipid interactions.

Another point about the salt bridges is that the bent-half simulation has the highest number of salt bridges, among our simulations. SP-B in bent-half simulation produce K24-D59 (Fig. 7, green and red lines) salt bridge similar to bent-in structure, R52-E51 and R36-E51 (Fig. 7, pink line) salt bridges similar to open structures, and R64-D59 (Fig. 7, blue) salt bridge, which is common for both open and bent structures. This could indicate the reason for similarities in the residue distance plots of the bent-half structure with open-in and open-half structures (Fig. 2), which could suggest the bent-half structure as the transition state between transmembrane orientations and open structures.

## 4. Discussion and conclusions

Obtaining information on equilibrium properties of biomolecular systems from molecular simulation is inherently challenging, given the many orders of magnitude in time separating atomic motions and different conformational changes undertaken by the protein. However, some proteins such as SP-B, that while are essential to life, have characteristics that make them particularly difficult to study experimentally. Thus, in order to provide a detailed insight into the basic structural properties of SP-B interacting with lipid bilayers, we have performed 2–2.5  $\mu\text{s}$  all-atom simulations of SP-B monomers in the presence of lipid, starting with 6 different initial system configurations. By the end of the simulations, these 6 configurations settle into 3 main SP-B/lipid topologies.

Time scales are always of concern in simulation. However, there exists a separation of time scales for different processes in membrane-protein systems [47]: equilibration of secondary structure occurs within 2  $\mu\text{s}$ , as does large structural change when there is a sizeable energetic driving force, while rearrangements between distinct tertiary structures

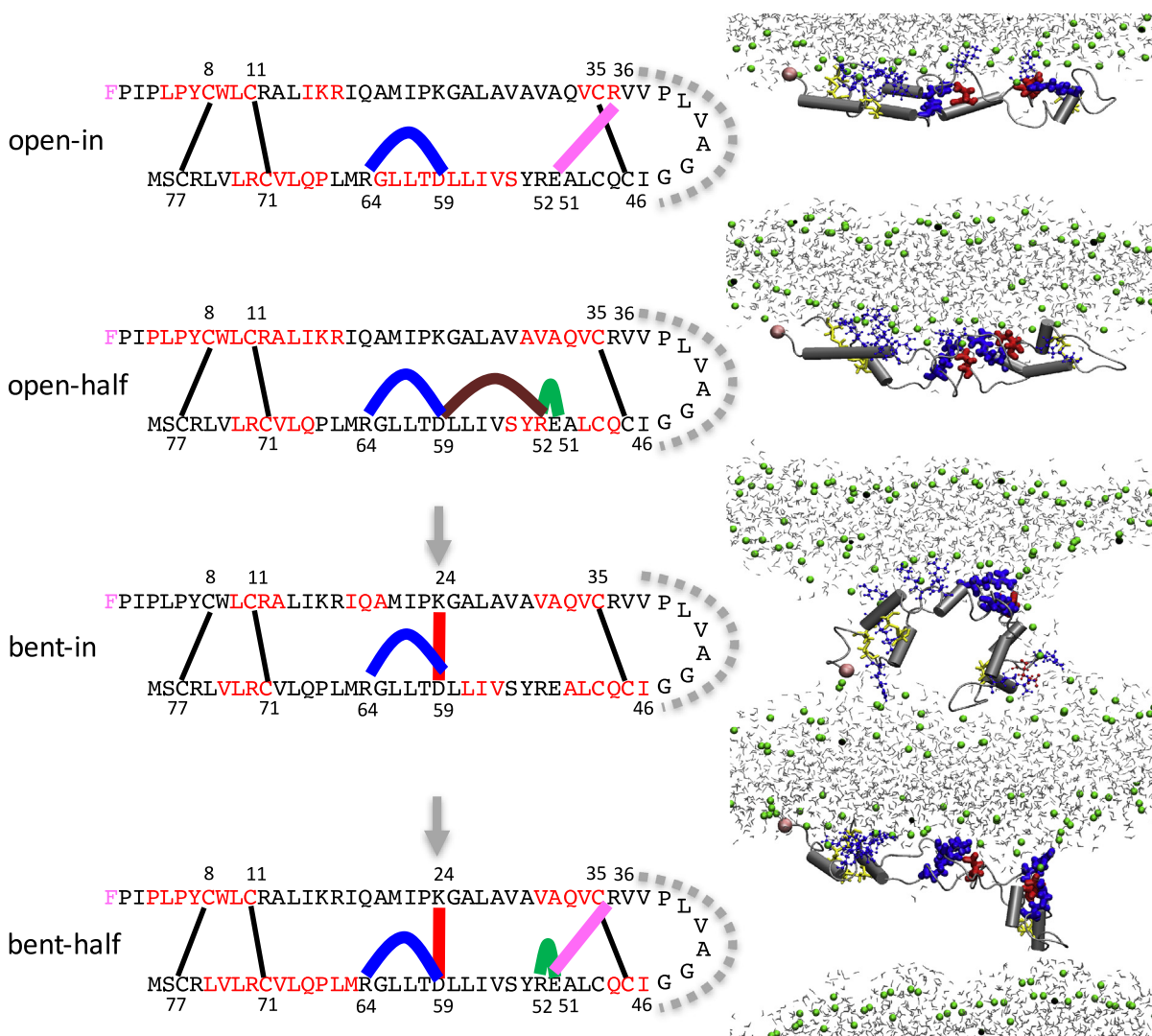


**Fig. 7.** Salt bridges in the final structures of SP-B for the in and half-in simulations. Here, we show a sequence representation of the protein (left) and a corresponding snapshot from near the end of the simulation (right). In the protein sequence, F1 is in pink, the helical regions are in red, the disulphide bonds are solid black lines and salt bridges are in colored bold lines (R64-D59 in blue, K24-D59 in red, R52-E51 in green, R36-E51 in pink and R52-D59 in brown). In the snapshots, F1 is in pink spheres, the protein backbone is in gray, the helical regions are in gray cylinders, negatively and positively charged residues are in red and blue, respectively with the salt-bridge-forming residues shown in licorice style, P atoms of lipid head group are in green spheres and water molecules are in silver lines. The last 200 ns of simulation are used for salt bridge calculations. 40% presence is chosen as the minimum to show the helicity and salt bridges. We used the default value of  $d \leq 3.2$  Å within VMD [46] to identify the salt bridges in our system. The gray arrows indicate the salt bridge that stabilizes the hinge of the bent structures. The thick dashed gray lines identify the loop region. (For interpretation of the references to color in this figure legend, the reader is referred to the web version of this article.)

separated by free energy barriers may take orders of magnitude longer. Gradual structural optimization of a particular conformation may also be very slow. While we have not fully equilibrated our systems, we do see secondary structure reaching a steady state (Fig. S.1) and significant larger-scale conformational changes: rapid closing of the bent-out configuration; the flattening of the initial bend in the bent-in and bent-half simulations; and the repeated flexing and straightening of the protein as the bent-half configuration interacts with the opposite leaflet (Fig. 6). We note also that the bent-half configuration has evolved to show very similar structure to the open-in and open-half simulations (see Fig. 2A, B and E), evidence that the open configuration represents a metastable state. The plots in Fig. S.2 showing protein position with respect to the membrane also generally settle into a steady state. Exceptions to this, apart from folding during the open-out simulation, are portions near the central loop for bent-in and bent-half that continue to drift to the opposing leaflet, which they may reach beyond  $\sim 10$   $\mu$ s. In terms of timescales required for insertion, we note that the bent-half configuration started partially inserted and entered fully into the membrane in approximately 1  $\mu$ s. Thus, the limiting step for insertion is the

free energy barrier associated with finding protein configurations that facilitate insertion, which our open-out and bent-out starting configurations clearly do not do.

In all cases, we find that the final overall percent helicity of SP-B is close to 35% (Fig. 4-C, D), which is consistent with experimental observations [19]. The N-terminal 7 residues of SP-B (the insertion sequence) has been shown experimentally to promote bilayer disruption [48] and nanosilos [49] and its deletion makes SP-B constructs less effective in biophysical assays of SP-B function [50]. These residues do not share homology with related saposin proteins and thus cannot be homology modeled, and so are often assumed to be without secondary structure. However, the simulations suggest that several of these residues can indeed take on a helical structure (Fig. 4-A, B). Also of note is the plasticity in the secondary structure of certain SP-B regions, which as discussed below, are associated with non-planar configurations of the protein that modify the structure of the bilayer. Experimentally, SP-B has been shown to be conformationally flexible and to exhibit different lipid binding modes for different preparation protocols [51,52]. Such conformational plasticity has precedent for saposin proteins – for

example saposin C has 5 distinct structures in protein data bank [10,11,12,18].

In our simulations, when SP-B is initially placed outside the bilayer, it rapidly collapses into a compact structure that interacts peripherally with the lipid bilayer using either of its hydrophilic faces. This is consistent with a potential SP-B mechanism that has been long proposed where SP-B keeps lipid multilayers in close proximity by simultaneously binding both adjacent lipid layers [53,54,55]. In earlier coarse-grained MARTINI simulations of Baoukina et al. [27] SP-B was seen to simultaneously bind to two lipid vesicles while outside the membrane.

When SP-B is initially placed completely or partially inside the bilayer, our simulations express two main energetically realistic conformations that SP-B can take on. The first of these is an open structure with all helices parallel to the lipid bilayer and the protein backbone positioned deeply within one leaflet of the bilayer, in keeping with the results of FTIR experiments which indicate an overall parallel orientation for SP-B [56]. In the second type of stable structure, some or all of SP-B's helices take on inclined orientations, i.e. orientations where they are not in the plane of the bilayer. The inclined regions of SP-B are associated with disruption of the bilayer to create and stabilize pore-like defects, characterized by the presence of lipid headgroups and water molecules in the membrane interior. It is

possible that such structures are behind the experimentally observed permeability of lipids in the presence of SP-B [57], although an alternate explanation has also been proposed to involve large SP-B multimers [24].

As discussed further below, SP-B's capability to reorganize lipid structures is of high interest with regards to understanding SP-B's functional mechanism in the lungs. Here, we note that the “hinge” that allows for bending of the overall structure of SP-B to induce/stabilize the lipid defect occurs at residues 21–24 and 63–66 (Fig. 7). In our simulations, the bend at the hinge is stabilized by a salt bridge from K24 to D59 that is present in the bent SP-B configurations but not in the open ones. Also of note with regards to SP-B's structural mechanism for pore formation, is the structural plasticity of the region around E51 (Fig. 7). Although homology modeling predicts this region to be helical, in our simulations it takes on quite a wide variety of secondary structures. And in particular when SP-B induces the formation of a pore, the helical structure in this region is broken, with the concomitant formation of salt bridges involving E51 and R52. Such salt bridges and consequently SP-B's ability to modify lipid bilayer structures may be affected by the nature of the lipid headgroups, and this implies a role in the local composition of the lipid membrane in the action of SP-B. In particular, while our simulations employed purely zwitterionic head groups, human lung surfactant has ~10% anionic lipids [1,2,3],

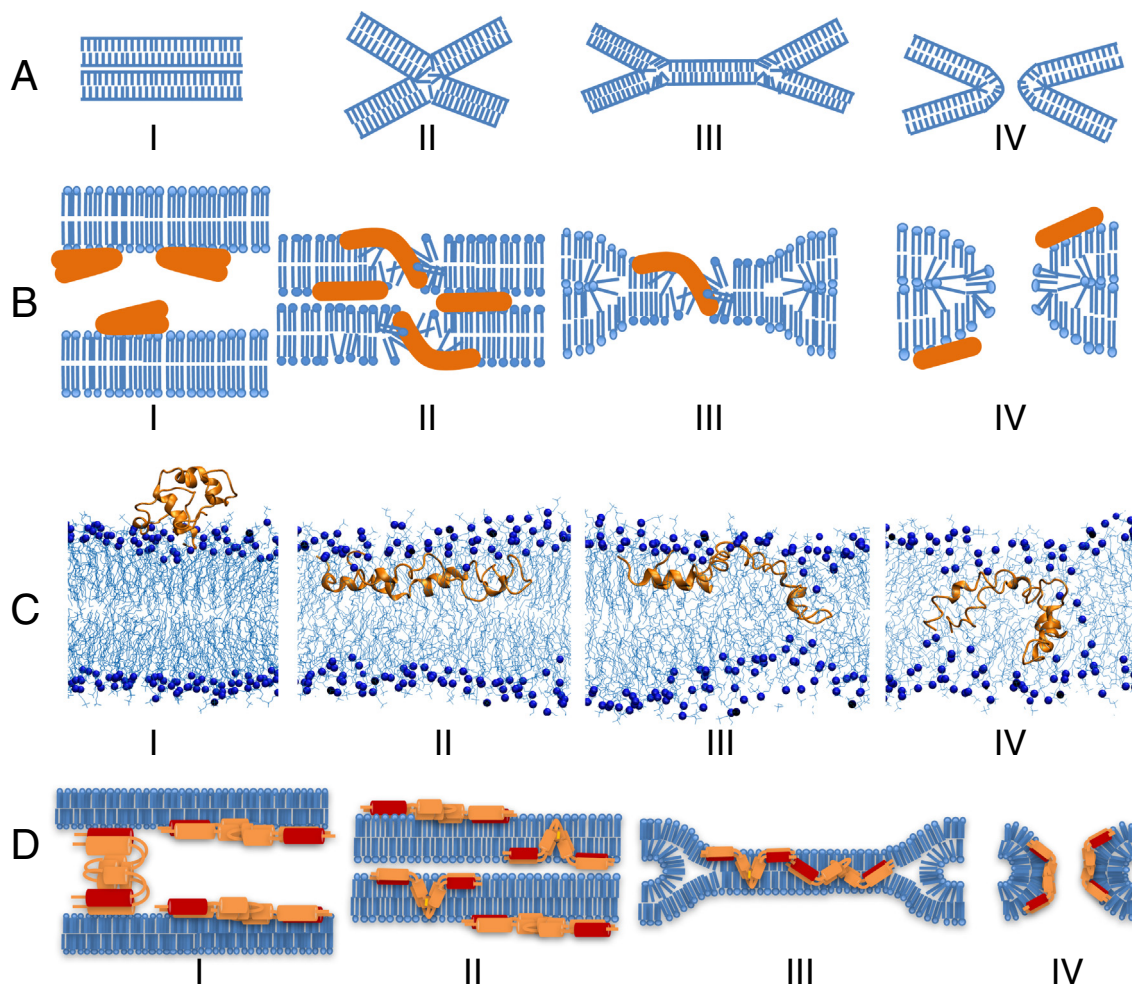


**Fig. 8.** Potential mechanism of SP-B induced fusion of two lipid bilayers suggested by the MD simulations. A) the four main steps of fusion: I) contact, II) stalk, III) diaphragm and IV) pore. B) a schematic view of how SP-B might promote these fusion steps: I) anchoring step by SP-B in a closed structure, II) lowering the energy barrier to help the bilayers form the stalk, III) the diaphragm step where SP-B can promote pore formation in the lipid bilayer and IV) complete pore. C) snapshots of SP-B simulations: I) outside the lipid bilayer helps to promote close contact between bilayers, II) in the open structure reduces the energy barrier, III and IV) generates and maintains the pore. D) speculative dimeric structures based on the SP-B monomers from the simulation and their potential lipid interactions. The red helix represents the N-terminal helix. (For interpretation of the references to color in this figure legend, the reader is referred to the web version of this article.)

which would compete for protein-protein R52 interactions. The central loop adjacent to E51, i.e. P39-L40-V41-A42-G43-G43, appears to be important in destabilizing the local lipid structures and exploring the opposing leaflet (Fig. 5), in order to initiate the formation of the defect. This capability may be aided by the disorder-promoting characteristics of proline and glycine, as well as the general hydrophobicity of the other residues in the loop. Of course it is important to keep in mind that our simulations were carried out purely with unsaturated lipids, while human lung surfactant normally contains ~40% saturated lipids [1,2,3], which means that our simulations may be biased towards seeing more non-planar lipid structures.

SP-B's activities in modifying lung surfactant lipid structures are at the center of its proposed mechanism(s) of action. SP-B is suggested to promote rapid adsorption of phospholipids to the interface from the aqueous subphase [54,58,59,60] and/or to promote the transfer of lipids to and from the monolayer at the air/water interface and the multilayers beneath [26,61,62,63]. In order to carry out such activities, it has been suggested that SP-B stabilizes a stalk or pore that bridges the gap between lipids at the surface and lipids in the hypophase beneath the surface. Thus, it is not surprising that SP-B's mechanism of action has often been considered in the light of the four canonical stages of membrane fusion (e.g. [8,22,26,53,64]) (Fig. 8–A). In Fig. 8, sequence A-I to A-IV, we present the four paradigmatic stages of membrane fusion: I) contact, II) stalk, III) diaphragm and IV) pore [65], respectively. Sequence B-I to B-IV of the same figure provides schematic representations of SP-B and how it may promote each stage, while sequence C-I to C-IV shows configurations from simulation that provide the motivation for the schematics. For contact (I), SP-B, possibly in a closed globular structure (while at the membrane surface), exposes hydrophilic residues that can “stick” to an incoming membrane and facilitate close contact. General disruption of the membrane by SP-B, especially by configurations tending towards a transmembrane positioning, facilitates both stalk (II) and diaphragm (III) formation. The ability of SP-B to form or to stabilize pores would obviously aid in the final stage (IV) of vesicle fusion. Although Fig. 8 shows only bilayer-bilayer interactions, both monolayer-bilayer and bilayer-bilayer interactions are important in lung surfactant and involve essentially the same SP-B/lipid interactions [66,67].

One important point to consider is the oligomerization state of SP-B. Native SP-B is thought to dimerize through C48, perhaps with additional stabilization through E51/R52 salt bridges [22,23], although deletion of C48 does not drastically impair SP-B's function [21]. SP-B may even function as a multimer of dimers [24]. Thus, we considered how dimerization via C48 would affect the SP-B structure and lipid interactions we observe in our simulations. In all final structures, C48 is well exposed and positioned to form interactions with another SP-B subunit (Fig. S.3). For the 3 main final SP-B structures, open, bent and closed, there are a number of plausible ways to form the dimers (Fig. S.4). As illustrated in Fig. 8–D, the dimer structures can maintain similar lipid- interactions as was seen in the monomer simulations. All atom simulations with dimeric SP-B will of course be of interest for a future study.

In summary, 2–2.5  $\mu$ s simulations using the OPLS-AA potential show that SP-B has reached energetically feasible structures and is stable in three main conformations: 1) open (parallel to but well embedded in a POPC lipid bilayer), 2) bent (produced and/or stabilized defects in the lipid bilayer), and 3) closed (peripherally associated with the lipid bilayer). In particular, we witness the central loop's ability to explore the opposite leaflet and to stabilize a pore-like structure, aided by its proline, glycine pair and hydrophobic residues. In all of this, structural plasticity and the presence of salt bridges are essential to SP-B interactions with the lipid bilayer.

### Transparency document

The Transparency document associated with this article can be found, in online version.

### Acknowledgments

Computations were performed on the GPC supercomputer at the SciNet HPC Consortium. SciNet is funded by: the Canada Foundation for Innovation under the auspices of Compute Canada; the Government of Ontario; Ontario Research Fund - Research Excellence; and the University of Toronto [68]. We acknowledge and thank Natural Sciences and Engineering Research Council of Canada (NSERC) for grants to VB (312676) and IS (205245), the Canadian Institutes for Health Research (CIHR) for the operating grant to VB (272291), as well as funding support from the Research and Development Corporation of Newfoundland (RDC) (5404-1030-106).

### Appendix A. Supplementary data

Supplementary data to this article can be found online at <http://dx.doi.org/10.1016/j.bbammem.2016.09.018>.

### References

- [1] A.D. Postle, E.L. Heeley, D.C. Wilton, A comparison of the molecular species compositions of mammalian lung surfactant phospholipids, *Comp. Biochem. Physiol. A Mol. Integr. Physiol.* 129 (1) (2001) 65–73.
- [2] J.N. Hildebran, J. Goerke, J. Clements, Pulmonary surface film stability and composition, *J. Appl. Physiol.* 47 (3) (1979) 604–611.
- [3] C.J. Lang, A.D. Postle, S. Orgeig, F. Possmayer, W. Bernhard, A.K. Panda, K. Jürgens, W.K. Milsom, K. Nag, C.B. Daniels, Dipalmitoylphosphatidylcholine is not the major surfactant phospholipid species in all mammals, *Am. J. Physiol. Regul. Integr. Comp. Physiol.* 289 (5) (2005) R1426–R1439.
- [4] J. Goerke, Pulmonary surfactant: functions and molecular composition, *Biochim. Biophys. Acta (BBA) - Mol. Basis Dis.* 1408 (2–3) (1998) 79–89.
- [5] F.X. McCormack, Structure, processing and properties of surfactant protein A, *Biochim. Biophys. Acta (BBA) - Mol. Basis Dis.* 1408 (2–3) (1998) 109–131.
- [6] E.C. Crouch, Structure, biologic properties, and expression of surfactant protein D (SP-D), *Biochim. Biophys. Acta (BBA) - Mol. Basis Dis.* 1408 (2–3) (1998) 278–289.
- [7] J. Johansson, Structure and properties of surfactant protein C, *Biochim. Biophys. Acta (BBA) - Mol. Basis Dis.* 1408 (2–3) (1998) 161–172.
- [8] S. Hawgood, M. Derrick, F. Poulain, Structure and properties of surfactant protein B, *Biochim. Biophys. Acta (BBA) - Mol. Basis Dis.* 1408 (2–3) (1998) 150–160.
- [9] J.C. Clark, S.E. Wert, C.J. Bachurski, M.T. Stahlman, B.R. Stripp, T.E. Weaver, J.A. Whitsett, Targeted disruption of the surfactant protein B gene disrupts surfactant homeostasis, causing respiratory failure in newborn mice, *Proc. Natl. Acad. Sci. U. S. A.* 92 (1995) 7794–7798.
- [10] C.A. Hawkins, E. de Alba, N. Tjandra, Solution structure of human saposin C in a detergent environment, *J. Mol. Biol.* 346 (2005) 1381–1392.
- [11] E. de Alba, S. Weiler, N. Tjandra, Solution structure of human saposin C: pH-dependent interaction with phospholipid vesicles, *Biochemistry* 42 (2003) 14729–14740.
- [12] V.E. Ahn, P. Leyko, J.R. Alattia, L. Chen, G.G. Prive, Crystal structures of saposins A and C, *Protein Sci.* 15 (2006) 1849–1857.
- [13] V.E. Ahn, K.F. Faull, J.P. Whitelegge, A.L. Fluharty, G.G. Prive, Crystal structure of saposin B reveals a dimeric shell for lipid binding, *Proc. Natl. Acad. Sci. U. S. A.* 100 (2003) 38–43.
- [14] E. Liepinsh, M. Andersson, J.M. Ruysschaert, G. Otting, Saposin fold revealed by the NMR structure of NK-lysin, *Nat. Struct. Biol.* 4 (1997) 793–795.
- [15] D.H. Anderson, M.R. Sawaya, D. Cascio, W. Ernst, R. Modlin, A. Krensky, D. Eisenberg, Granulysin crystal structure and a structure-derived lytic mechanism, *J. Mol. Biol.* 325 (2003) 355–365.
- [16] M. Leippe, H. Bruhn, O. Hecht, J. Grotzinger, Ancient weapons: the three-dimensional structure of amoebapore A, *Trends Parasitol.* 21 (2005) 5–7.
- [17] O. Hecht, N.A. Van Nuland, K. Schleinkofer, A.J. Dingley, H. Bruhn, M. Leippe, J. Grotzinger, Solution structure of the pore-forming protein of *Entamoeba histolytica*, *J. Biol. Chem.* 279 (2004) 17834–17841.
- [18] M. Rossmann, R. Schultz-Heienbrock, J. Behlke, N. Rimmel, C. Alings, K. Sandhoff, W. Saenger, T. Maier, Crystal structures of human saposins C and D: implications for lipid recognition and membrane interactions, *Structure* 16 (2008) 809–817.
- [19] B. Olmeda, B. García-Alvarez, J. Perez-Gil, Structure-function correlations of pulmonary surfactant protein SP-B and the saposin-like family of proteins, *Eur. Biophys. J.* 42 (2–3) (2013) 209–222.
- [20] M. Sarker, A.J. Waring, F.J. Walther, K.M. Keough, V. Booth, Structure of mini-B, a functional fragment of surfactant protein B, in detergent micelles, *Biochemistry* 46 (39) (2007) 11047–11056.
- [21] D.C. Beck, M. Ikegami, N. Cheng-Lun, S. Zaltash, J. Johansson, J.A. Whitsett, T.E. Weaver, The role of homodimers in surfactant protein B function in vivo, *J. Biol. Chem.* 275 (2000) 3365–3370.
- [22] S. Zaltash, M. Palmblad, T. Curstedt, J. Johansson, B. Persson, Pulmonary surfactant protein B: a structural model and a functional analogue, *Biochim. Biophys. Acta* 1466 (1–2) (2000) 179–186.

- [23] S. Zaltash, W. Griffiths, C.D. Beck, C.X. Duan, T.E. Weaver, J. Johansson, Membrane activity of (Cys48Ser) lung surfactant protein B increases with dimerisation, *Biol. Chem.* 382 (6) (2001).
- [24] B. Olmeda, B. Garcia-Alvarez, M.J. Gomez, M. Martinez-Calle, A. Cruz, J. Perez-Gil, A model for the structure and mechanism of action of pulmonary surfactant protein B, *FASEB J.* 29 (10) (2015) 4236–4247.
- [25] F.J. Walther, A.J. Waring, J.M. Hernandez-Juviel, L.M. Gordon, Z. Wang, C.L. Jung, P. Ruchala, A.P. Clark, W.M. Smith, S. Sharma, R.H. Notter, Critical structural and functional roles for the N-terminal insertion sequence in surfactant protein B analogs, *PLoS One* 5 (1) (2010) e8672.
- [26] S. Baoukina, D.P. Tieleman, Direct simulation of protein-mediated vesicle fusion: lung surfactant protein B, *Biophys. J.* 99 (7) (2010) 2134–2142.
- [27] S. Baoukina, D.P. Tieleman, Lung surfactant protein SP-B promotes formation of bilayer reservoirs from monolayer and lipid transfer between the interface and sub-phase, *Biophys. J.* 100 (7) (2011) 1678–1687.
- [28] S. Altschul, W. Gish, W. Miller, E. Myers, D. Lipman, Basic local alignment search tool, *J. Mol. Biol.* 215 (3) (1990) 403–410.
- [29] A. Drozdetskiy, C. Cole, J. Procter, G.J. Barton, JPred4: a protein secondary structure prediction server, *Nucleic Acids Res.* 43 (2015) W389–W394.
- [30] 01 08 2016 [Online]. Available: <http://www.compbio.dundee.ac.uk/jpred/>.
- [31] N. Guex, M.C. Peitsch, SWISS-MODEL and the Swiss-PdbViewer: an environment for comparative protein modeling, *Electrophoresis* 18 (15) (1997) 2714–2723.
- [32] D. Palloboina, A.J. Waring, R.H. Notter, V. Booth, M. Morrow, Effects of the lung surfactant protein B construct Mini-B on lipid bilayer order and topography, *Eur. Biophys. J.* 41 (9) (2012) 755–767.
- [33] A. Johansson, T. Curstedt, Molecular structures and interactions of pulmonary surfactant components, *Eur. J. Biochem.* 244 (3) (1997) 675–693.
- [34] M.H. Khatami, M. Bromberek, I. Saika-Voivod, V. Booth, Molecular dynamics simulations of histidine-containing cod antimicrobial peptide paralogs in self-assembled bilayers, *Biochim. Biophys. Acta Biomembr.* 1838 (11) (2014) 2778–2787.
- [35] M.G. Wolf, M. Hoefling, C. Aponte-Santamaria, H. Grubmuller, G. Groenhof, "g-memmed: Efficient Insertion of a Membrane Protein into an Equilibrated Lipid Bilayer with Minimal Perturbation," *J. Comput. Chem.* 31 (11) (2010) 2169–2174.
- [36] W.L. Jorgensen, D.S. Maxwell, J. Tirado-Rives, Development and testing of the OPLS all-atom force field on conformational energetics and properties of organic liquids, *J. Am. Chem. Soc.* 118 (45) (1996) 11225–11236.
- [37] G.A. Kaminski, R.A. Friesner, Evaluation and reparametrization of the OPLS-AA force field for proteins via comparison with accurate quantum chemical calculations on peptides, *J. Phys. Chem. B* 105 (28) (2001) 6474–6487.
- [38] D.P. Tieleman, J.L. Maccallum, W.L. Ash, C. Kandt, Z. Xu, L. Monticelli, Membrane protein simulations with a united-atom lipid and all-atom protein model: lipid-protein interactions, side chain transfer free energies and model proteins, *J. Phys. Condens. Matter* 18 (28) (2006) 1221–1234.
- [39] W. Humphrey, A. Dalke, K. Schulten, VMD: visual molecular dynamics, *J. Mol. Graph.* 14 (1996) 33–38.
- [40] [Online]. Available: <http://www.ks.uiuc.edu/Research/vmd/> (Accessed 27 02 2014).
- [41] D. Frishman, P. Argos, Knowledge-based protein secondary structure assignment, *Proteins Struct. Funct. Genet.* 23 (1995) 566–579.
- [42] G.W. Touw, C. Baakman, J. Black, T.A.H. te Beek, E. Krieger, R.P. Joosten, G. Vriend, A series of PDB-related databanks for everyday needs, *Nucleic Acids Res.* 43 (2015) D364–D368.
- [43] W. Kabsch, C. Sander, Dictionary of protein secondary structure: pattern recognition of hydrogen-bonded and geometrical features, *Biopolymers* 22 (12) (1983) 2577–2637.
- [44] B.A. Reva, A.V. Finkelstein, J. Skolnick, What is the probability of a chance prediction of a protein structure with an rmsd of 6 Å? *Fold. Des.* 3 (2) (1998) 141–147.
- [45] V.N. Maiorov, G.M. Crippen, Significance of root-mean-square deviation in comparing three-dimensional structures of globular proteins, *J. Mol. Biol.* 235 (1994) 625–634.
- [46] [Online]. Available: <http://www.ks.uiuc.edu/Research/vmd/plugins/saltbr/> (Accessed 12 09 2015).
- [47] Y. Wang, T. Zhao, D. Wei, E. Strandberg, A.S. Ulrich, J.P. Ulmschneider, How reliable are molecular dynamics simulations of membrane active antimicrobial peptides? *Biochim. Biophys. Acta Biomembr.* 1838 (9) (2014) 2280–2288.
- [48] M. Sharifahmadian, M. Sarker, D. Palloboina, A.J. Waring, F.J. Walther, M.R. Morrow, V. Booth, Role of the N-terminal seven residues of surfactant protein B (SP-B), *PLoS One* 8 (9) (2013) e72821.
- [49] S.L. Frey, L. Pociavsek, A.J. Waring, F.J. Walther, J.M. Hernandez-Juviel, P. Ruchala, K.Y. Lee, Functional importance of the NH2-terminal insertion sequence of lung surfactant protein B, *Am. J. Physiol. Lung Cell. Mol. Physiol.* 298 (3) (2010) 335–347.
- [50] A.G. Serrano, M. Ryan, T.E. Weaver, J. Pérez-Gil, Critical structure-function determinants within the N-terminal region of pulmonary surfactant protein SP-B, *Biophys. J.* 90 (1) (2006) 238–249.
- [51] A. Cruz, C. Casals, J. Pérez-Gil, Conformational flexibility of pulmonary surfactant proteins SP-B and SP-C, studied in aqueous organic solvents, *Biochim. Biophys. Acta* 1255 (1) (1995) 68–76.
- [52] J. Pérez-Gil, A. Cruz, C. Casals, Solubility of hydrophobic surfactant proteins in organic solvent/water mixtures. Structural studies on SP-B and SP-C in aqueous organic solvents and lipids, *Biochim. Biophys. Acta* 1168 (3) (1993) 261–270.
- [53] A.G. Serrano, J. Pérez-Gil, Protein-lipid interactions and surface activity in the pulmonary surfactant system, *Chem. Phys. Lipids* 141 (1–2) (2006) 105–118.
- [54] A. Cruz, C. Casals, K.M.W. Keough, J. Pérez-Gil, Different modes of interaction of pulmonary surfactant protein SP-B in phosphatidylcholine bilayers, *Biochem. J.* 327 (1997) 133–138.
- [55] R. Chang, S. Nir, F.R. Poulain, Analysis of binding and membrane destabilization of phospholipid membranes by surfactant apoprotein B, *Biochim. Biophys. Acta Biomembr.* 1371 (2) (1998) 254–264.
- [56] G. Vandenbussche, A. Clercx, M. Clercx, T. Curstedt, J. Johansson, H. Jornvall, J.M. Ruyschaert, Secondary structure and orientation of the surfactant protein SP-B in a lipid environment. A fourier transform infrared spectroscopy study, *Biochemistry* 31 (1992) 9169–9176.
- [57] E. Parra, A. Alcaraz, A. Cruz, V.M. Aguilera, J. Pérez-Gil, Hydrophobic pulmonary surfactant proteins SP-B and SP-C induce pore formation in planar lipid membranes: evidence for proteolipid pores, *Biophys. J.* 104 (2013) 146–155.
- [58] J. Pérez-Gil, K.M. Keough, Interfacial properties of surfactant proteins, *Biochim. Biophys. Acta* 1408 (2–3) (1998) 203–217.
- [59] F. Possmayer, K. Naga, K. Rodriguez, R. Qanbar, S. Schürch, Surface activity in vitro: role of surfactant proteins, *Comp. Biochem. Physiol. A Mol. Integr. Physiol.* 129 (1) (2001) 209–220.
- [60] A. Cruz, D. Marsh, J. Pérez-Gil, Rotational dynamics of spin-labelled surfactant-associated proteins SP-B and SP-C in dipalmitoylphosphatidylcholine and dipalmitoylphosphatidylglycerol bilayers, *Biochim. Biophys. Acta* 1415 (1998) 125–134.
- [61] L.A.J.M. Creuwels, E.H. Boer, R.A. Demel, L.M.G.v. Golde, H.P. Haagsman, Neutralization of the positive charges of surfactant protein C. Effects on structure and function, *J. Biol. Chem.* 270 (1995) 16225–16229.
- [62] M. Ross, S. Krol, A. Janshoff, H.J. Galla, Kinetics of phospholipid insertion into monolayers containing the lung surfactant proteins SP-B or SP-C, *Eur. Biophys. J.* 31 (2002) 52–61.
- [63] M.A. Oosterlaken-Dijksterhuis, H.P. Haagsman, L.M. van Golde, R.A. Demel, Characterization of lipid insertion into monomolecular layers mediated by lung surfactant proteins SP-B and SP-C, *Biochemistry* 30 (45) (1991) 10965–10971.
- [64] J. Pérez-Gil, Structure of pulmonary surfactant membranes and films: the role of proteins and lipid-protein interactions, *Biochim. Biophys. Acta Biomembr.* 1778 (7–8) (2008) 1676–1695.
- [65] L.V. Chernomordik, M.M. Kozlov, Mechanics of membrane fusion, *Nat. Struct. Mol. Biol.* 15 (2008) 675–683.
- [66] E. Parra, J. Pérez-Gil, Composition, structure and mechanical properties define performance of pulmonary surfactant membranes and films, *Chem. Phys. Lipids* 185 (2015) 153–175.
- [67] Y.Y. Zuo, R.A. Veldhuizen, A.W. Neumann, N.O. Petersen, F. Possmayer, Current perspectives in pulmonary surfactant-inhibition, enhancement and evaluation, *Biochim. Biophys. Acta* 1778 (10) (2008) 1947–1977.
- [68] C. Loken, D. Gruner, L. Groer, R. Peltier, N. Bunn, M. Craig, T. Henriques, J. Dempsey, C. Yu, J. Chen, L.J. Dursi, J. Chong, S. Northrup, J. Pinto, N. Knecht, R. van Zon, SciNet: lessons learned from building a power-efficient Top-20 system and data centre, *J. Phys. Conf. Ser.* 256 (2010) 1.